Noninvasive *in vivo* spectroscopic nanorod-contrast photoacoustic mapping of sentinel lymph nodes

Kwang Hyun Song[1], Chulhong Kim[2], Konstantin Maslov[1], Lihong V. Wang[*]

Department of Biomedical Engineering, Washington University in St. Louis, Campus Box 1097, One Brookings Drive, St. Louis, MO 63130-4899, United States

ARTICLE INFO

ABSTRACT

Sentinel lymph node (SLN) biopsy has increasingly become important in axillary staging of breast cancer patients since SLN biopsy alleviates the postoperative complications of previously practiced axillary lymph node dissections. Nevertheless, the procedures of SLN biopsy using blue dye and radioactive substance are still intraoperative, and the latter methods are also ionizing. In this pilot study, we have proposed noninvasive *in vivo* spectroscopic photoacoustic (PA) SLN mapping using gold nanorods as lymph node tracers in a rat model. Gold nanorods have biocompatibility, high optical absorption, and easily tuned surface plasmon resonance peak wavelength.

1. Introduction

Sentinel lymph node biopsy (SLNB) has become an axillary staging routine for breast cancer patients as an alternative to traditional axillary lymph node dissection (ALND) [1]. Sentinel lymph nodes (SLNs) are defined as the first draining lymph nodes. Metastatic cancer cells tend to orderly progress out of the original cancer site through the SLNs [1,2]. In ALND, 10 or more lymph nodes are resected. By contrast, in SLNB, only the SLNs are biopsied to determine whether further lymph node dissection is necessary or not [3]. If the SLNs are cancer-free, the chances are low that the other lymph nodes are affected; thus, no more lymph node dissection is necessary. SLNB has become a standard procedure in axillary staging because it has less invasiveness and side effects than ALND. Furthermore, ALND does not improve the survival rate in comparison to SLNB while causing significant morbidity, such as lymphedema, limitations of arm and shoulder movement, and numbness in the upper arm.

In SLNB, blue dye (methylene blue or isosulfan blue) and radioactive isotope materials (^{99m}Tc) are administered near the cancer 5 min and 24 h before a surgery, respectively [2–4]. The injected tracers flow to the SLNs via the lymphatic system. The accumulated blue dye is visually detected through the surgery, while radioactive substances are detected by a Geiger counter [5]. Since blue

dye molecules are small and can easily migrate to adjacent lymph nodes passing the SLNs, the blue dye-based method alone may have a high false positive rate [6,7]. Because radioactive isotope materials are bigger ($\sim$500 nm), the method using these substances is expected to have less migration to echelon lymph nodes. However, those bigger colloids are mostly retained in the interstitial space and significantly less accumulated in the lymph nodes [1]. Moreover, this method not only has poor spatial resolution, making SLN mapping difficult, but also uses harmful ionizing radioactive materials, which cause damage on connective tissues and also require a special facility to produce.

These complications initiated studies to find safe, noninvasive, and high-resolution SLN mapping methods, avoiding invasive surgeries and allowing minimally invasive staging by such as needle biopsy. Optical imaging is one of such methods because it is safe and non-ionizing. Further, it is more sensitive to imaging contrast than other conventional imaging methods, such as magnetic resonance imaging (MRI), X-ray computed tomography (X-ray CT), and positron emission tomography (PET). Therefore, near-infrared fluorescent type II quantum dots have been used as optical lymph node tracers and successfully applied to map SLNs in an animal model [8]. However, because of strong light scattering, this kind of purely optical imaging techniques based on diffuse light detections suffer from poor spatial resolution beyond the quasi-diffusive regime [9]. To overcome the poor spatial resolution, hybrid imaging modalities such as photoacoustic (PA) imaging, have been implemented by detecting ultrasound instead of light [10]. In PA imaging, a short pulsed laser illuminates biological tissue. Optical absorbers in the tissue absorb optical energy and expand because of thermo-elastic expansion, generating ultrasonic waves. As a result, PA imaging inherits high optical contrast and excellent ultrasonic spatial

* Corresponding author. Tel.: +1 314 935 6152; fax: +1 314 935 7448.
E-mail addresses: ksong@biomed.wustl.edu (K.H. Song),
chkim@biomed.wustl.edu (C. Kim), kimaslov@biomed.wustl.edu (K. Maslov),
lhwang@biomed.wustl.edu (L.V. Wang).
[1] Tel.: +1 314 935 4911; fax: +1 314 935 7448.
[2] Tel.: +1 314 935 9587; fax: +1 314 935 7448.

(A)

(B)
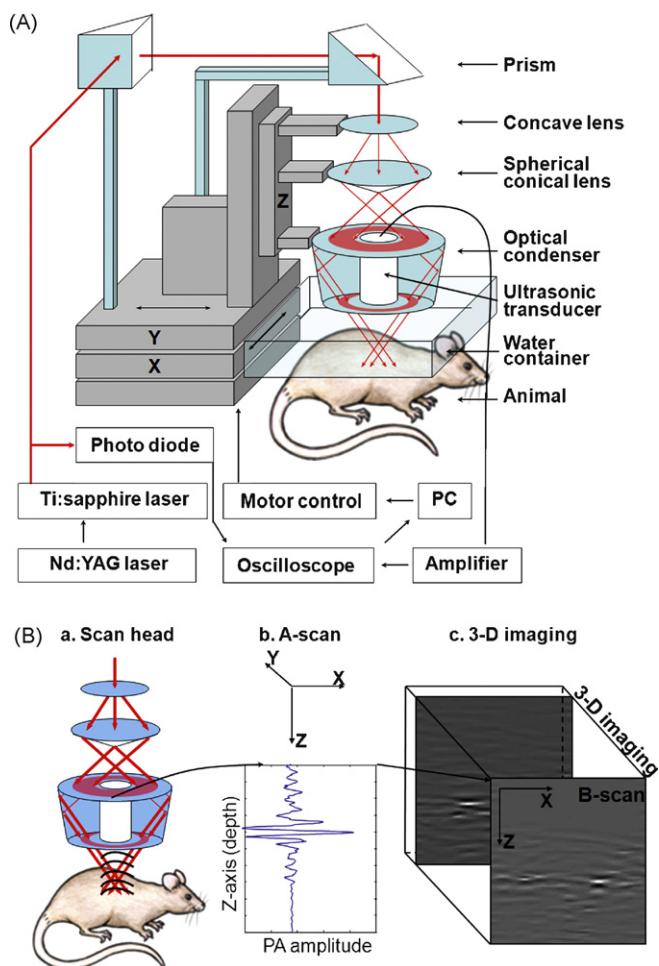
Fig. 1. (A) Schematic of a deeply penetrating reflection-mode photoacoustic imaging system. (B) Image formation. A-scan: 1-D image and B-scan: 2-D image. A B-scan is composed of multiple A-scans. Multiple B-scans form a 3-D image. PA: photoacoustic.

resolution. Because PA imaging uses multiply scattered photons, it has fairly deep imaging depth while maintaining satisfactory spatial resolution [10,11]. The modality has been successfully employed to image various biological structures of small animals [10,12] and also extended to clinical studies [13].

In this study, we have successfully mapped a SLN using spectroscopic photoacoustic imaging using gold nanorods in a rat model. Similar to other metal nanoparticles, gold nanorods have 5 orders of magnitude higher molar optical absorption than conventional absorbing dye molecules [14]. In addition, the surface plasmon resonance (SPR) peak wavelength of nanorods can be easily tuned because that depends on the shape, mainly on the aspect ratio of the axial diameter to the longitudinal length [14]. We showed that the gold nanorods can be used as new lymph node tracers. In addition, to identify the SLN out of blood vessels without taking a control image before the injection of tracers, we have proposed a spectroscopic PA mapping method.

2. Materials and methods

2.1. Photoacoustic imaging system

The PA imaging system is schematically described in Fig. 1A. The system was designed to image deeply located biological structures [10]. For PA excitation, a Ti:sapphire laser (LT-2211A, LOTIS TII) pumped by a Q-switched Nd:YAG (LS-2137/2, LOTIS TII) laser

was employed. The laser system has a 10 Hz pulse-repetition rate and about 10 ns pulse width. The laser beam with high optical energy was delivered to an object through two prisms and three optical parts. The three optical parts—a concave lens, a spherical conical lens, and an optical condenser—were employed to form ring-shaped illumination. Such dark-field illumination reduces unwanted surface PA signal generation, which otherwise overshadows PA signals generated from a deep region [10]. For spectroscopic PA imaging, wavelengths of 757 nm, 807 nm, and 820 nm from the tunable Ti:sapphire laser were chosen. The laser beam was sufficiently broadened to satisfy the ANSI safety limit (actual fluence: 6.9 mJ/cm^2, limit: 31 mJ/cm^2) [15].

For raster scanning, a motorized XY linear translation stage (XY-6060, Danaher Motion) was used, which was controlled by a computer. For Z directional (depth) adjustment of the scan head, another linear translation stage (KR-20, THK) was employed. Scanning stepsizes for a 1-D scan (X direction) and for a 2-D scan (XY directions) were 0.2 mm and 0.4 mm, respectively. With the current laser system, the total acquisition time for a 25 mm × 30 mm field of view was 23 min.

Three-dimensional data was acquired by the raster scanning (Fig. 1B). At a given point, a time-resolved PA signal was received by an ultrasonic transducer (Fig. 1Ba). This PA signal was then converted to a depth-resolved signal by multiplying the time by the speed of sound (Fig. 1Bb). The depth-resolved PA signal is called an A-scan, which is a 1-D image. Once multiple A-scans are acquired with 1-D scanning (X direction), a B-scan (2-D image) was obtained (Fig. 1Bc). Similarly, multiple B-scans compose a 3-D image with another 1-D scanning (Y direction). Although the 3-D image can be viewed in various forms, it is here expressed in the form of maximum amplitude projection (MAP), which projects the maximum of each A-scan onto the corresponding XY coordinate.

For PA signal detection, a 5 MHz central frequency ultrasonic transducer (V308, Panametrics-NDT) was used, which has a 2.54 cm focal length, a 1.91 cm aperture, and a 72% nominal bandwidth at full width at half maximum (FWHM). With the transducer, the axial resolution and the transverse resolution at 19 mm deep were about 144 μm and 560 μm, respectively [10]. The resolutions were experimentally measured by imaging human hairs in scattering medium. The transducer mechanically scanned an object in a water container through a bottom opening (5 cm × 5 cm), which was sealed with a thin and clear membrane. The object was placed below the water
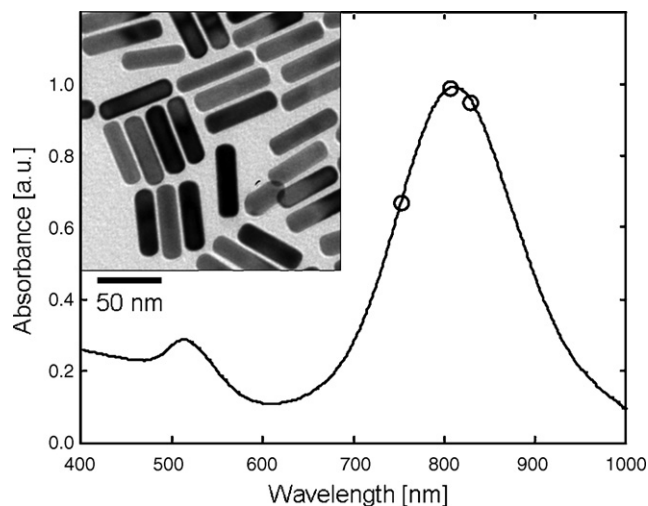
Fig. 2. Absorbance of gold nanorods. Diameter: 10 nm; length: 41 nm; and a SPR peak wavelength: 807 nm. Normalized values are presented. Circles represent the wavelengths used for spectroscopic photoacoustic SLN mapping. Inset is a TEM image of the gold nanorods.
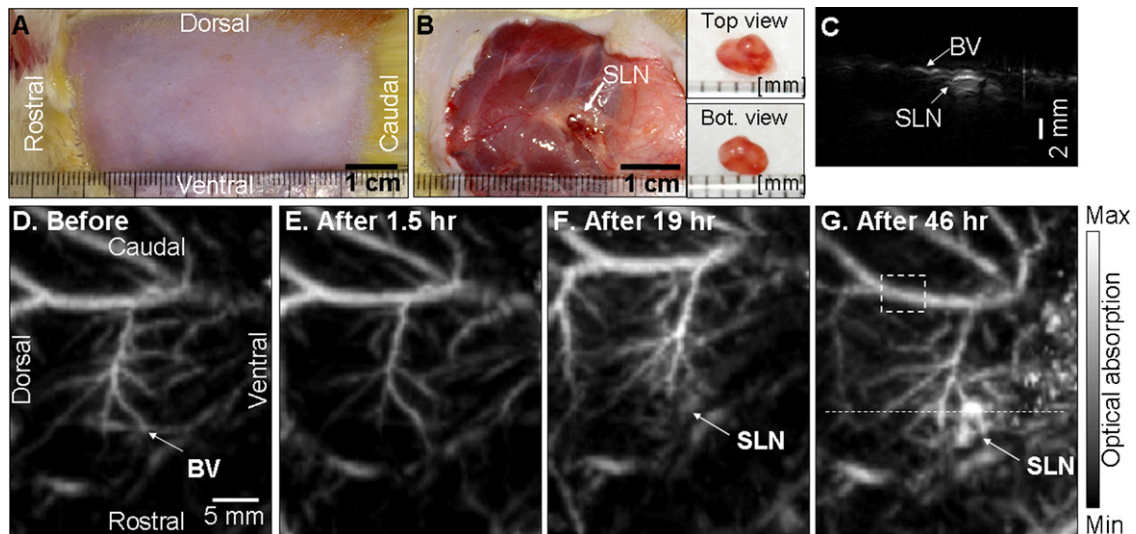
Fig. 3. A sagittal photoacoustic MAP image of the axilla, showing the vasculature and sentinel lymph node. (A) Photograph of the region of interest with hair removed before imaging. (B) Anatomical photograph of the axilla with skin and fatty tissue removed. Sentinel lymph node is indicated by an arrow. Insets are a top view and a bottom view of the dissected sentinel lymph node, respectively. (C) B-scan acquired at the dotted line in (G). (D) Photoacoustic MAP image acquired before the injection, showing the axillary vasculature. (E) Photoacoustic MAP image taken 1.5 h after the injection. (F) Photoacoustic MAP image acquired at 19 h after the injection. (G). Photoacoustic MAP image acquired at 46 h after the injection. The sentinel lymph node appears slightly in (F) and strongly in (G).

container. To couple ultrasound between the transducer and the object, ultrasonic gel (Sonotec Inc.) was applied between the object and the membrane. Received PA signals were amplified by an amplifier (5072PR, Panametrics-NDT), digitized by an oscilloscope (TDS 5054, Tektronix), and then stored in the computer. Since the laser system has pulse-to-pulse fluctuations in energy, the PA signals were corrected by signals from a photodiode, which measures the energy of the original laser beam.

2.2. Animal and drug information

Adult male Sprague Dawley rats weighing ∼400 g were used. Before depilation in the axillary region, a mixture of ketamine (85 mg/kg) and xylazine (15 mg/kg) was administered in a rat. After the hair removal, the rat was put sideway on an animal holder. During all image acquisitions, the rat was kept under anesthesia with a vaporized-isoflurane system (1 L/min oxygen and 0.75% isoflurane, Euthanex Corp.) while the vitals were monitored by a pulse oximeter (NONIN Medical Inc., 8600V). For hydration, 1 ml of 0.9% saline was subcutaneously administered between image acquisitions.

As lymph node tracers, gold nanorods (Nanopartz Inc.) were injected on a left forepaw pad in the amount of 0.1 ml at a 979-pM concentration [16]. The gold nanorods used for this study have a 10 nm diameter, a 41 nm length, and an 807 nm SPR peak wavelength. Fig. 2 shows the shape and the absorbance spectrum of gold nanorods used for this study. After data acquisition, the animal was euthanized by a pentobarbital overdose. All animal experiments were carried out in compliance with the guidelines on the care and the use of laboratory animals from Washington University in St. Louis.

3. Results

Noninvasive *in vivo* PA SLN mapping with gold nanorods has been successfully accomplished in a rat model. An axillary region of a rat shown in Fig. 3A was scanned with the PA imaging system. Fig. 3B is an anatomical photograph taken after all image acquisitions, with the skin and surrounding fatty tissue removed, revealing a SLN. Insets are photographs of a top view and a bottom view of the dissected SLN, in which the nanorod-accumulated parts are in red color. Before the injection of the gold nanorods, a PA image was
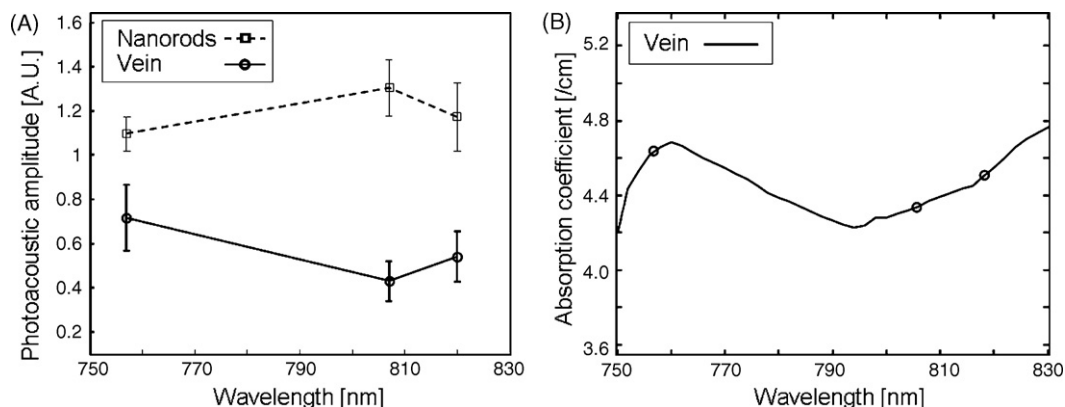
Fig. 4. (A) Photoacoustic amplitude versus the wavelengths from the nanorods (sentinel lymph node) and the venous vessel. Squares with dotted lines indicate the PA signals from the nanorods. Circles with solid lines represent the PA signals from the venous vessel. Error bar represents standard error. (B) Absorption coefficient of 70% oxygenated hemoglobin in venous vessel. Circles indicate the wavelengths used for the spectroscopic measurement.

acquired as a control to be compared with images taken after the injection. The control image was then processed to form a sagittal MAP image (Fig. 3D). The vasculature of the axilla was clearly imaged with good contrast. After the injection of the gold nanorods on the left forepaw pad of the rat, we obtained consecutive PA images until the SLN appears clearly in the image. Fig. 3E is a sagittal PA MAP image acquired 1.5 h after the injection, where no SLN is visible. At 19 h after the injection, the SLN was barely seen with a low contrast (Fig. 3F). At 46 h after the injection, the SLN was clearly imaged with good contrast (Fig. 3G). One of the B-scans (Fig. 3C) acquired at the dotted line in Fig. 3G provides depth information of the SLN and the blood vessels. The average depth of the SLNs of rats weighing ~400 g is about 1.5 mm from the skin surface. In the B-scan image, the skin surface is not seen clearly because the high contrast signal of the SLN suppresses the low contrast signal of the skin.

If the above method were used to identify a SLN, a control image has to be acquired before the injection, and then an after-injection image was compared with the control image. However, if the technique is to be extended to the clinic, it is inconvenient to acquire a control image. In addition, if we do not have prior information about the vascular morphology in an axillary region, we cannot separate the SLN out of blood vessels. Therefore, a spectroscopic PA method using 757 nm, 807 nm, and 820 nm wavelengths was applied to identify the SLN, avoiding the need of acquiring a control image. Fig. 4A shows the changes of the PA amplitudes versus the wavelengths in the SLN and the blood vessel. As expected, the PA amplitudes (squares with dotted lines) obtained from the SLN reach the maximum at the 807 nm wavelength, which is the SPR peak wavelength of the gold nanorods. The PA amplitudes follow the absorbance curve of the gold nanorods (Fig. 2). By contrast, the PA amplitudes (circles with solid lines) acquired from the blood vessel (dotted box in Fig. 3G) follow the absorption coefficient curve of 70% oxygenated hemoglobin in veins (Fig. 4B) [17]. Circles in Fig. 4B indicate the wavelengths used for the spectroscopic PA imaging.

4. Discussion

We demonstrated the feasibility of noninvasive *in vivo* PA SLN mapping by injecting gold nanorods into rats. In a lymphatic system, it is well known that smaller sized nanoparticles (<5 nm) migrate to SLNs faster than larger nanoparticles [5]. Methylene blue, which has a 0.7 nm in diameter and a 1.6 nm in length [6], takes 5 min to reach SLNs in humans. Radioactive isotope, ^{99m}Tc (~1000 nm), takes up to 24 h. Spherical nanoparticles of 40 nm in diameter take about 4.6 min to reach SLNs of rats [18]. Here, we observed that the gold nanorods with a 10 nm diameter and a 41 nm length took more than 20 h to reach the SLNs. The reticuloendothelial cells might react differently to nanoparticles of different shapes. Further biological study will be needed to understand this phenomenon. Another aspect affecting the accumulation time is the surface condition of the nanorods for the lymphatic system. The nanorods used for this study are plain nanoparticles, so phagocytosis occurs actively in extracellular space, and hence slower drainage. PEGylation can improve the drainage rate of nanoparticles since this process changes the surface condition of the nanorods from hydrophobic to hydrophilic, resulting in less phagocytosis in extracellular space [19] and aggregation at the injection site [20].

The nanoparticles injected into the body are removed by reticuloendothelial systems, such as monocytes and macrophages. In addition, their long-term toxicity is still studied in various research groups. To reduce any potential toxicity, it is recommended to minimize the dosage of nanoparticles. In this study, the minimum dosage detectable by the PA system was estimated based on the acquired images. Since the detection limit of the system is about 10 dB and the SNR of the SLN is about 34 dB, the dosage can be roughly reduced by a factor of 15.

We have also proposed the spectroscopic method to separate SLNs out of blood vessels without obtaining a control image. As seen in Fig. 4A, the SLN could be separated from the blood vessel because the optical absorption spectra of both nanorods and hemoglobin have different profiles. Although the PA amplitude variations at the three wavelengths are small because of the small wavelength difference between the selected wavelengths compared to the broad spectrum of the nanorods, the profile of the nanorods (squares with the dotted lines) is distinct from the profile of the vein (circles with the solid lines). In the blood vessel, which is labeled vein in Fig. 4A, the spectral profile does not follow the one of the gold nanorods, but follow the absorption spectrum of 70% oxygenated hemoglobin in a vein. Thus, this blood vessel is considered to be a venous blood vessel.

Owing to the wavelength-dependent optical attenuation in the skin, the optical fluence reaching the SLNs is also wavelength-dependent. This effect on the SLN region should be corrected to produce accurate spectra of PA amplitudes. In this study, we compensated the PA signals using the diffusion equation with experimentally measured effective attenuation coefficients of the rat skin. To measure the effective attenuation coefficients, a highly absorptive object (a carbon rod) with an absorption coefficient independent of the wavelength was inserted below the skin of a rat. PA signals were then measured over multiple wavelengths [21]. The PA signals are proportional to specific optical absorption at the carbon rod, which reflects the relative spectral dependence of the optical fluence.

Since the imaging system employs a single ultrasonic transducer and the pulse-repetition rate of the laser system is limited to 10 Hz, the total acquisition time for a 25 mm × 30 mm field of view was 20 s and 23 min for 2-D (B-scan) and 3-D imaging, respectively. Artifacts due to breathing motions were unavoidable. If we employ an ultrasonic array system and a faster pulse-repetition-rate laser system, the breathing motion effect can be minimized. A breathe-gating system will also be able to reduce the motion artifact. These systems can also reduce the amplitude variations of PA signals between image acquisitions, possibly caused by breathing motion (focal zone effect) and physiological variations (concentration and oxygenation of hemoglobin) of the animal.

In summary, noninvasive PA SLN mapping using gold nanorods has been successfully accomplished. Gold nanorods possess several orders of magnitude higher molar optical absorption than conventional dye, and their optical absorption peak wavelength can be easily tuned to the spectral window of low optical attenuation in tissue by changing the aspect ratio. In addition, gold material is biocompatible. We demonstrated that gold nanorods can be good optical lymph node tracers. To make the PA SLN mapping more practical, we have also proposed a spectroscopic method. With this method, we could identify the SLN out of blood vessels. The proposed spectroscopic mapping method can potentially be extended to the clinic with the aid of a faster acquisition system.

References

[1] Alazraki NP, Eshima D, Eshima LA, et al. Lymphoscintigraphy, the sentinel node concept, and the intraoperative gamma probe in melanoma, breast cancer, and other potential cancers. Semin Nucl Med 1997;27(1):55–67.

[2] McMasters KM, Tuttle TM, Carlson DJ, et al. Sentinel lymph node biopsy for breast cancer: a suitable alternative to routine axillary dissection in multi-institutional practice when optimal technique is used. J Clin Oncol 2000;18(13): 2560–6.

[3] Kobayashi H, Kawamoto S, Sakai Y, et al. Lymphatic drainage imaging of breast cancer in mice by micro-magnetic resonance lymphangiography using a nano-size paramagnetic contrast agent. J Natl Cancer Inst 2004;96(9): 703–8.

[4] Bass SS, Cox CE, Ku NN, et al. The role of sentinel lymph node biopsy in breast cancer. J Am Coll Surg 1999;189(2):183–94.

[5] Soltesz EG, Kim S, Laurence RG, et al. Intraoperative sentinel lymph node mapping of the lung using near-infrared fluorescent quantum dots. Ann Thorac Surg 2005;79(1):269–77 [discussion 269–277].

[6] Sohrabnezhad S, Pourahmad A, Sadjadi MA. New methylene blue incorporated in mordenite zeolite as humidity sensor material. Mater Lett 2007;61(11–12):2311–4.

[7] Torchia MG, Nason R, Danzinger R, et al. Interstitial MR lymphangiography for the detection of sentinel lymph nodes. J Surg Oncol 2001;78(3):151–6 [discussion 157].

[8] Kim S, Lim YT, Soltesz EG, et al. Near-infrared fluorescent type II quantum dots for sentinel lymph node mapping. Nat Biotechnol 2004;22(1):93–7.

[9] Parungo CP, Colson YL, Kim SW, et al. Sentinel lymph node mapping of the pleural space. Chest 2005;127(5):1799–804.

[10] Song KH, Wang LV. Deep reflection-mode photoacoustic imaging of biological tissue. J Biomed Opt 2007;12(6):060503.

[11] Ku G, Wang LV. Deeply penetrating photoacoustic tomography in biological tissues enhanced with an optical contrast agent. Opt Lett 2005;30(5):507–9.

[12] Oh JT, Li ML, Zhang HF, et al. Three-dimensional imaging of skin melanoma in vivo by dual-wavelength photoacoustic microscopy. J Biomed Opt 2006;11(3): 34032.

[13] Manohar S, Vaartjes SE, van Hespen JCG, et al. Initial results of in vivo non-invasive cancer imaging in the human breast using near-infrared photoacoustics. Opt Express 2007;15(19):12277–85.

[14] Jain PK, Lee KS, El-Sayed IH, et al. Calculated absorption and scattering properties of gold nanoparticles of different size, shape, and composition: applications in biological imaging and biomedicine. J Phys Chem 2006;110(14):7238–48.

[15] American National Standards Institute. American National Standard for the Safe Use of Lasers ANSI Z136.1-2000. New York; 2000.

[16] Yang X, Skrabalak SE, Li ZY, et al. Photoacoustic tomography of a rat cerebral cortex in vivo with au nanocages as an optical contrast agent. Nano Lett 2007;7(12): 3798–802.

[17] Jacques SL, Prahl SA. Absorption spectra for biological tissues; 2008. http://omlc.ogi.edu/spectra/hemoglobin/index.html.

[18] Nakajima M, Takeda M, Kobayashi M, et al. Nano-sized fluorescent particles as new tracers for sentinel node detection: experimental model for decision of appropriate size and wavelength. Cancer Sci 2005;96(6):353–6.

[19] Otsuka H, Nagasaki Y, Kataoka K. PEGylated nanoparticles for biological and pharmaceutical applications. Adv Drug Deliv Rev 2003;55(3):403–19.

[20] Moghimi SM, Bonnemain B. Subcutaneous and intravenous delivery of diagnostic agents to the lymphatic system: applications in lymphoscintigraphy and indirect lymphography. Adv Drug Deliv Rev 1999;37(1–3):295–312.

[21] Li M-l, Oh J-t, Xie X, et al. Simultaneous molecular and hypoxia imaging of brain tumors in vivo using spectroscopic photoacoustic tomography. In: Proceedings of IEEE. 2007.